



**HAL**  
open science

# Surface Modification of 3D-Printed Micro- and Macro-Structures via In Situ Nitroxide-Mediated Radical Photopolymerization

Xingyu Wu, Benjamin Leuschel, Nguyen Hoai Nam, Yohann Guillaneuf,  
Didier Gimes, Jean-louis Clément, Arnaud Spangenberg

► **To cite this version:**

Xingyu Wu, Benjamin Leuschel, Nguyen Hoai Nam, Yohann Guillaneuf, Didier Gimes, et al.. Surface Modification of 3D-Printed Micro- and Macro-Structures via In Situ Nitroxide-Mediated Radical Photopolymerization. *Advanced Functional Materials*, In press, 10.1002/adfm.202312211 . hal-04407799

**HAL Id: hal-04407799**

**<https://hal.science/hal-04407799>**

Submitted on 21 Jan 2024

**HAL** is a multi-disciplinary open access archive for the deposit and dissemination of scientific research documents, whether they are published or not. The documents may come from teaching and research institutions in France or abroad, or from public or private research centers.

L'archive ouverte pluridisciplinaire **HAL**, est destinée au dépôt et à la diffusion de documents scientifiques de niveau recherche, publiés ou non, émanant des établissements d'enseignement et de recherche français ou étrangers, des laboratoires publics ou privés.

# Surface Modification of 3D-Printed Micro- and Macro-Structures via In Situ Nitroxide-Mediated Radical Photopolymerization

Xingyu Wu,\* Benjamin Leuschel, Nguyen Hoai Nam, Yohann Guillaneuf, Didier Gignes, Jean-Louis Clément, and Arnaud Spangenberg\*

Photo-controlled reversible-deactivation radical polymerization (RDRP) has recently emerged in light-based 3D printing at macro- and micro-scales, enabling the elaboration of objects with (re-)configurable surface properties. The authors' previous work exploits nitroxide-mediated radical photopolymerization (NMP2) in 3D micro-printing and subsequent surface modification, by employing analkoxyamine-based photoresist via 3D direct laser writing (DLW). However, this photoresist suffers from its low photosensitivity to wavelengths above 760 nm, limiting its suitability for commercial 3D DLW setups. To tackle these issues, a new strategy—in situ NMP2 based on a photoresist containing a commercial photoinitiator and a photosensitive-nitroxide is proposed. This photoresist is well-suited for wavelengths commonly used by 3D DLW systems to obtain well-defined 3D microstructures. Importantly, the in-situ formation of alkoxyamine during fabrication allows photo-induced surface modification of microstructures, highlighted by precise and successive surface patterning. The surface modification can be conducted at 800 nm or at wavelengths up to 860 nm. Subsequently, the impact of light wavelength and intensity is investigated to understand surface modification. The simple preparation of this novel photoresist allows facile adaptation to digital light processing for 3D macro-printing. This work broadens the scope of photo-controlled RDRP in 3D printing and greatly facilitates “living” 3D micro- and macro-printing.

photopolymerization, allowing the creation of complex and high-resolution 3D objects.<sup>[1]</sup> In order to adapt 3D objects to advanced applications such as tissue engineering, microfluidics, and electronics,<sup>[2]</sup> besides their topological design, it is highly desirable to control surface properties and functionalities of 3D structures, particularly in a spatiotemporally precise manner.<sup>[3]</sup> However, most photopolymerization reactions employed in 3D printing are conventional free radical polymerizations, resulting in polymeric networks consisting of “dead” chains after printing, due to irreversible termination reactions (e.g., radical combination and disproportionation), thus limiting the introduction of new chemical compositions and further new properties.<sup>[1d,4]</sup> An elegant method for spatially controlled, covalent surface functionalization is to change chemical components involved in polymer network formation to render it chemically addressable after 3D printing.<sup>[3b,5]</sup> For example, the integration of photoenol groups into the network allows the use of maleimides for surface modification upon light irradiation.<sup>[3b,5b,6]</sup>

## 1. Introduction

Light-based 3D printing generally involves converting reactive liquid resins into solid materials by spatiotemporally controlled

Yet, notably, customizing surface functionalization of 3D objects for a wide variety of demands remains challenging.

Recently, an advanced polymer synthesis technique—photo-controlled RDRP—has emerged in 3D printing and opened new

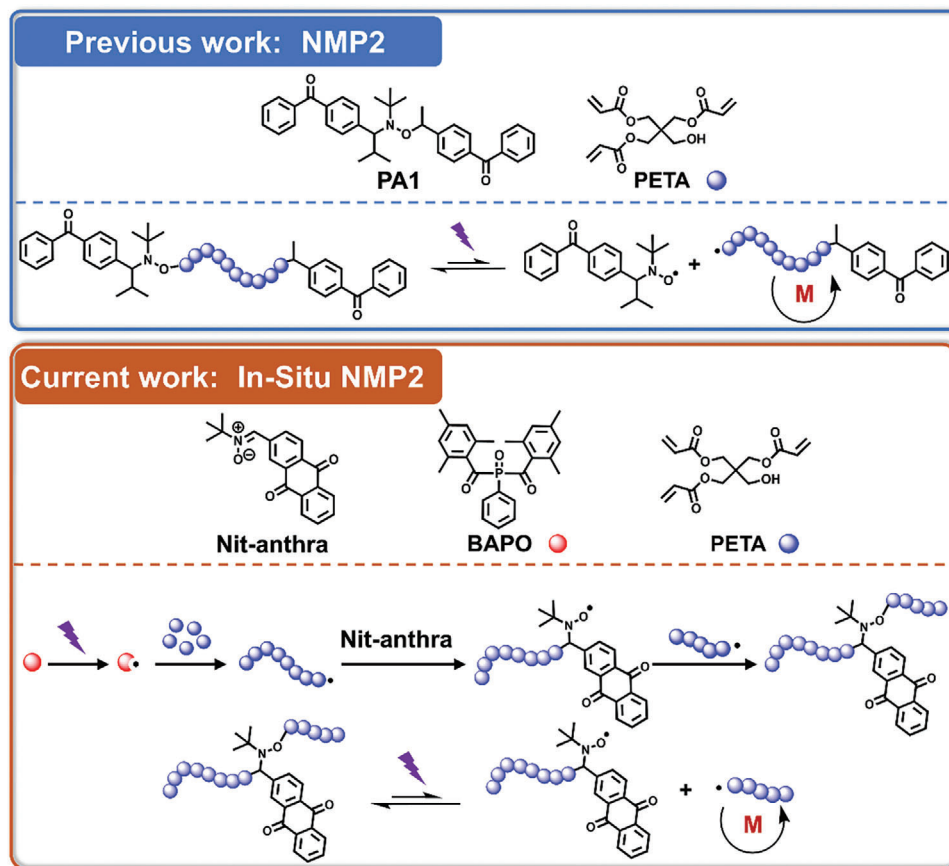
X. Wu, B. Leuschel, A. Spangenberg  
Institut de Science des Matériaux de Mulhouse (IS2M)  
CNRS—UMR 7361  
Université de Haute-Alsace  
15 rue Jean Starcky, Mulhouse 68057, France  
E-mail: x53.wu@qut.edu.au; arnaud.spangenberg@uha.fr

 The ORCID identification number(s) for the author(s) of this article can be found under <https://doi.org/10.1002/adfm.202312211>

© 2023 The Authors. Advanced Functional Materials published by Wiley-VCH GmbH. This is an open access article under the terms of the [Creative Commons Attribution-NonCommercial](https://creativecommons.org/licenses/by-nc/4.0/) License, which permits use, distribution and reproduction in any medium, provided the original work is properly cited and is not used for commercial purposes.

DOI: 10.1002/adfm.202312211

X. Wu, B. Leuschel, A. Spangenberg  
Université de Strasbourg  
Strasbourg 67000, France  
N. H. Nam, Y. Guillaneuf, D. Gignes, J.-L. Clément  
Aix Marseille Univ  
CNRS  
Institut de Chimie Radicale  
Aix-Marseille Université  
Marseille F-13397, France



**Scheme 1.** Top: chemical structure of the photoresist components (alkoxyamine [PA1] and PETA) employed in the previous work and the mechanism of NMP2 (ref. [11a]). Bottom: chemical structures of the photoresist components (Nit-anthra, BAPO, and PETA) used in the current work and the proposed mechanism of in situ NMP2 consisting of spin trapping process of macroradicals followed by NMP2.

opportunities for 3D printing and surface functionalization.<sup>[7]</sup> In a pioneering work, Bagheri et al. employed photoiniferter reversible addition-fragmentation chain-transfer (RAFT) polymerization in Digital Light Processing (DLP), and the successful post-printing monomer insertion demonstrated the retention of RAFT functionalities, that is, the “living” characteristics of polymer chains, within the 3D-printed polymer network.<sup>[8]</sup> Later, alternative strategies were reported, including photoinduced electron/energy transfer-RAFT polymerization (by Jin, Boyer, and colleagues) and Norrish type I photoinitiated RAFT polymerization (by Boyer and co-workers) in DLP 3D printing in order to improve printing speed and conduct printing under air.<sup>[9]</sup> Moreover, the outstanding spatially resolved surface functionalization demonstrated the ability of photo-controlled RAFT polymerization for tailoring the surface properties of 3D-printed macrostructures.<sup>[9d]</sup> Very recently, our group pioneered the use of photo-controlled RAFT polymerization in 3D DLW and opened a new perspective of photo-controlled RDRP in 3D printing.<sup>[10]</sup> Importantly, this work highlighted that the “living” characteristics of polymer chains formed by photo-RAFT polymerization enable the versatile reconfiguration of microstructures’ surfaces across multiple layers and using different materials via DLW.

Recent works have further extended the development of “living” 3D printing from photo-controlled RAFT polymerization to other types of photo-controlled RDRP, such as atom transfer radical polymerization (ATRP) and nitroxide-mediated radical polymerization (NMP).<sup>[11]</sup> Our previous work explored nitroxide-mediated radical photopolymerization (NMP2) in 3D DLW by employing an alkoxyamine-based photoresist and succeeded to spatially control the surface properties of microstructures via DLW (see **Scheme 1**, top).<sup>[11a]</sup> However, as noted, this photoresist can only access DLW at wavelengths below 760 nm, due to its low photo-sensitivity, which in turn significantly restricting its use in commercial 3D printing setups based on two-photon polymerization (e.g., Nanoscribe, Up Nano, ...).

In order to tackle these problems and to further explore NMP2 in 3D printing, in our present work, a new strategy—in situ NMP2—is proposed, based on a novel photosensitive system consisting of a commercial photoinitiator and a photosensitive nitroxide. After introducing this system into a photoresist, well-defined 3D microstructures can be obtained via 3D DLW employing commonly used wavelengths for irradiation. Remarkably, during printing, the photoresist enables the in situ formation of alkoxyamine, which can subsequently be photo-activated for

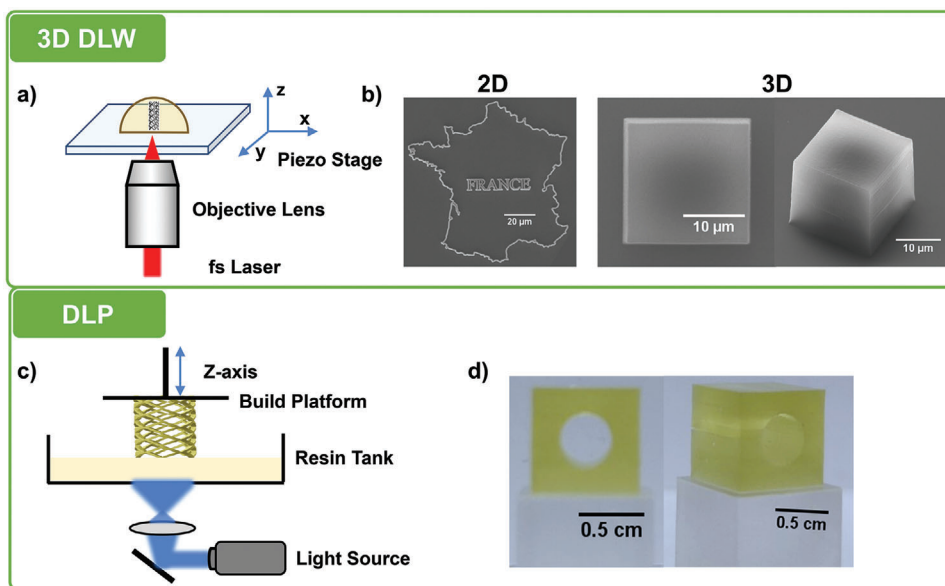


**Figure 1.** a) Schema of DLW 3D printing; b) SEM image of a 2D France map ( $800\text{ nm}$  and  $5.15\text{ mW cm}^{-2}$ ) and a cube (top view and  $45^\circ$  tilt view;  $800\text{ nm}$  and  $7.84\text{ mW cm}^{-2}$ ) made by 3D DLW; c) Schema of DLP 3D printing; d) Photographs of a printed hollow cube ( $385\text{ nm}$ ,  $5\text{ mW cm}^{-2}$ , and  $7\text{ s}$  per layer) printed via DLP. Formulation: PETA + Nit-anthra (2 wt%) + BAPO (2 wt%).

precise, successive surface modification. The impact of various writing parameters, including wavelength and laser intensity on the surface modification is investigated to allow further optimization of surface modification. Additionally, our photoresist can be adapted to DLP for 3D macro-printing and surface functionalization, benefiting from its simple preparation and facile scaling-up.

## 2. Results and Discussion

### 2.1. Chemical Structures and In Situ NMP2 Mechanism

The photoresist was developed by adding a nitron (called herein Nit-anthra) and phenyl bis(2,4,6-trimethylbenzoyl) phosphine oxide (BAPO) into pentaerythritol triacrylate (PETA)—a functional monomer commonly used in 3D printing. The chemical structures of these compounds are shown in the bottom of Scheme 1. BAPO is a commercially available photoinitiator and has excellent accessibility to 3D DLW and DLP set-ups. Nit-anthra is employed as a spin trapping agent, leading to a macro-nitroxide that could act as a controlling agent. Its synthesis process is detailed in the Supporting Information and its chemical structure was verified via  $^1\text{H}$  NMR and  $^{13}\text{C}$  NMR (Figure S1, Supporting Information). As illustrated in Scheme 1 (bottom part), upon light irradiation, the photolysis of a photoinitiator (here, BAPO) generates free radicals, enabling the initiation of polymerization of monomers to form macroradical chains. Reacting with a spin trapping agent (here, Nit-anthra), these macroradicals forms stable radical trap adducts—macro-nitroxides—and subsequent quenching of these macro-nitroxides by propagating chains forms macro-alkoxyamine, which in turn enables subsequent NMP2 to incorporate other monomers and functionalities. In situ NMP2—in situ alkoxyamine-formation process based on spin capturing<sup>[12]</sup> together with the NMP2 process<sup>[13]</sup>—

sets a solid foundation for 3D printing and light-controlled surface modifications.

### 2.2. 3D Micro- and Macro-Structures and Surface Modification

3D DLW, based on two-photon polymerization, has gained prominence to create arbitrary and high-resolution microstructures.<sup>[1b,e,2e,14]</sup> To investigate our photoresist's performance in 3D DLW (the setup is illustrated in Figure 1a), a map of France (2D) and a cube (3D) were fabricated at  $\lambda = 800\text{ nm}$  with a laser intensity of  $5.15$  and  $7.84\text{ mW cm}^{-2}$ , respectively. A detailed description of the fabrication setup and process is available in the Supporting Information. The SEM images in Figure 1b clearly show that these structures have well-defined shapes and sub-micrometer feature sizes ( $\approx 500\text{ nm}$  for the map). It should be pointed out that this photoresist can be facilely adapted to 3D DLW with wavelength above  $760\text{ nm}$ , which is a big advantage over our previously developed alkoxyamine-based photoresist, which cannot be employed to generate microstructures upon irradiation above  $760\text{ nm}$  due to its low photosensitivity. Besides,  $800\text{ nm}$  being a commonly used wavelength in 3D DLW, the excellent performance of our photoresist at this wavelength makes it promising for application in commercial 3D DLW set-ups using near-infrared excitation (e.g., Nanoscribe or Up Nano). In addition, in contrast to the preparation of the alkoxyamine-based photoresist, the current photoresist is easy to prepare and scale up, ascribed to the use of a commercial photoinitiator and the simple synthesis of the nitron, making it possible to be used in 3D macro-printing setups, such as DLP.

DLP forms 3D structures layer by layer through ultraviolet (UV) irradiation. It has attracted much attention due to its capability for rapid production of 3D objects and affordable pricing.<sup>[1h,15]</sup> Here, a commercial DLP printer (Asiga Pico2 HD)

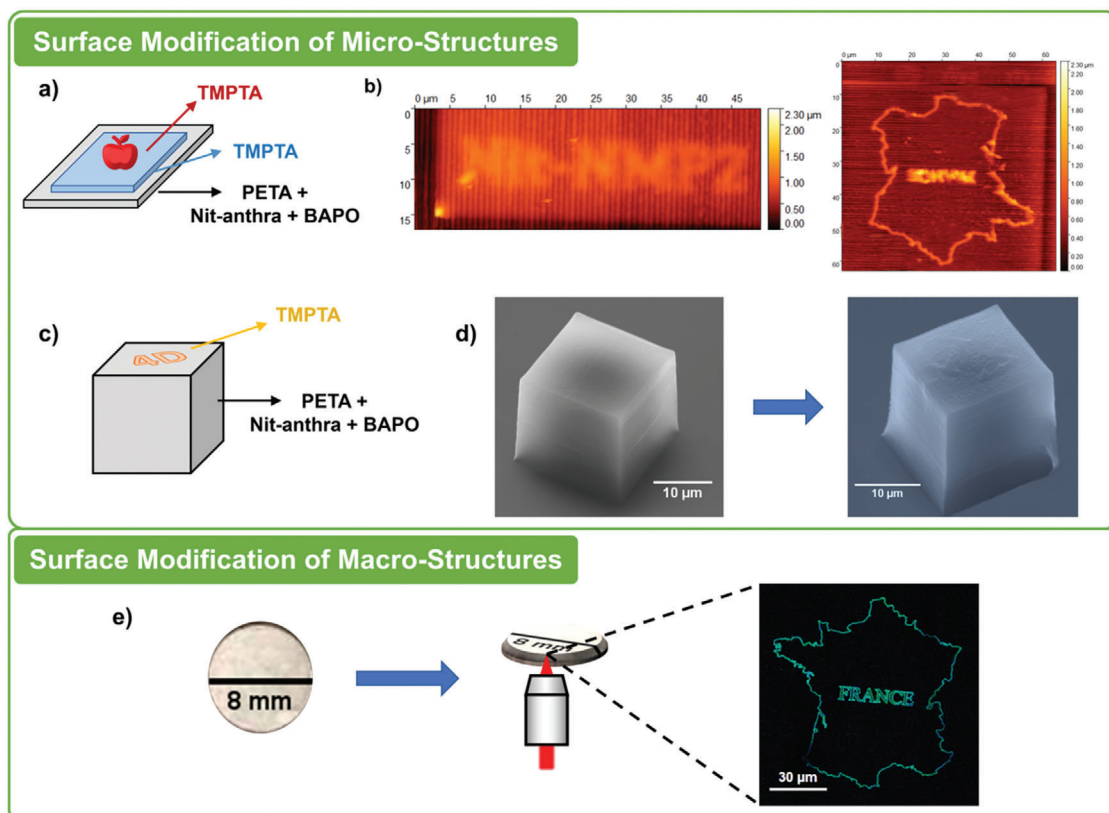


**Figure 2.** a) Illustration of surface modification on a stack of two squares; b) AFM images of Nit-NMP2 logo and map of France on the top of the second square (Base square made from PETA + Nit-anthra [2 wt%] + BAPO [2 wt%] at 800 nm and  $7.10 \text{ mW cm}^{-2}$ ; second square made from TMPTA alone at 800 nm and  $8.02 \text{ mW cm}^{-2}$  under  $\text{N}_2$ ; Logo and map made from TMPTA alone at 800 nm and  $12.37 \text{ mW cm}^{-2}$  under  $\text{N}_2$ ); c) Illustration of surface modification of 3D structures; d) Left: SEM images of a cube (see Figure 1b). Right: SEM images of functionalized cube (4D was made from TMPTA alone; 800 nm and  $12.21 \text{ mW cm}^{-2}$ ); e) Illustration of surface modification of macrostructures, with a photograph of a round piece made from PETA + Nit-anthra (2 wt%) + BAPO (2 wt%) at 385 nm,  $5 \text{ mW cm}^{-2}$ , and 5 s. Right: FLIM image of the round piece modified with France map (made from TMPTA + Rhodamine B at 800 nm and  $11.39 \text{ mW cm}^{-2}$ ).

equipped with a 385 nm UV LED projector was used (illustrated in Figure 1c). A hollow cube was designed and fabricated (Figure 1d) to demonstrate the potential of our formulation in 3D macro-printing. According to the Jacobs working curve of the photoresist (Figure S2, Supporting Information),  $5 \text{ mW cm}^{-2}$  and 7 s per layer was chosen as the key printing parameters, permitting high resolution under a relatively fast printing speed. A detailed explanation of the Jacobs working curve and of the selection of printing parameters is provided in the Supporting Information. The printed structure has a well-defined hollow shape and low surface roughness, indicating the adaptability of our photoresist to DLP and 3D macro-printing, in addition to 3D micro-printing.

Our formulation exhibits good printability at both micro- and macro-scales. Importantly, the in situ formed macroalkoxyamine during printing allows the introduction of new monomers for surface functionalization, which will be discussed afterward.

Prior to surface functionalization, an irradiated solution of Nit-anthra + BAPO + PETA was studied by electron paramagnetic resonance (EPR). Under light irradiation (405 nm), the appearance of an anisotropic EPR signal that is characteristic of nitroxide species (see Figure S3, Supporting Information) confirms the

in situ formation of the macro-nitroxide by spin trapping (as discussed above), which paves the way toward the success of surface functionalization. It has to be mentioned that anisotropic shape of the EPR signal is very likely due to the structure of the macro-nitroxide and the increase of the viscosity in the media both limiting the motion of nitroxide. Surface functionalization experiments were carried out in a 3D DLW setup, the same as that used for 3D micro-printing. As shown in Figure 2a, surface patterns were fabricated at the top of a stack of two squares using a resin—trimethylolpropane triacrylate (TMPTA)—without the addition of photoinitiators at  $12.37 \text{ mW cm}^{-2}$  and 800 nm. The base square was made using our photoresist (Nit-anthra + BAPO + PETA) at  $7.10 \text{ mW cm}^{-2}$  ( $\lambda = 800 \text{ nm}$ ), whereas the second square—on the top of the base square—is a functional layer made from TMPTA alone at  $8.02 \text{ mW cm}^{-2}$  ( $\lambda = 800 \text{ nm}$ ). AFM images show these well-defined patterns on the top (Figure 2b), the Nit-NMP2 logo and the map of France, demonstrating the precise spatial control of photo-induced surface modification conferred by our new strategy—in situ NMP2. The detailed surface modification processes are provided in the Supporting Information. It is worth pointing out that the surface modification can be achieved across multiple layers using monomers alone without the addition of photoinitiators, indicating the chain growth on the surface via

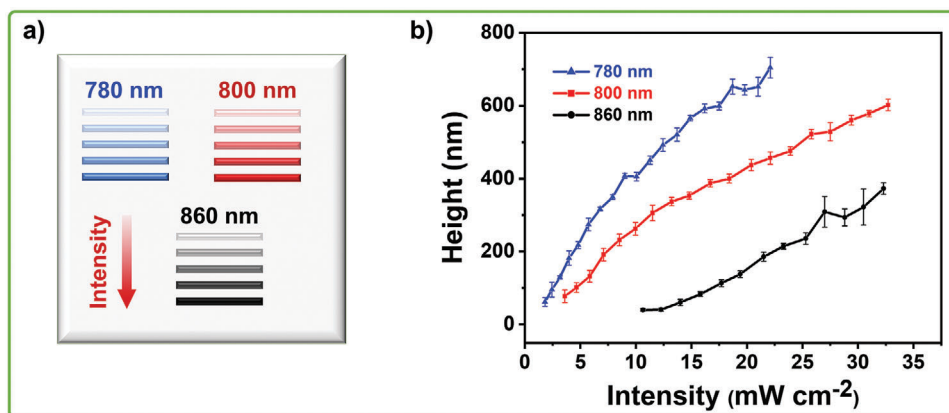


**Figure 3.** a) Schematic illustration of surface modifications to study the impact of the wavelength used for modification; b) Heights of lines fabricated at different intensities, made from TMPTA alone at 780, 800, and 860 nm under  $N_2$ . The first layer is a square made at  $5.15 \text{ mW cm}^{-2}$  at 800 nm (PETA + Nit-anthra [2 wt%] + BAPO [2 wt%]).

NMP thanks to the in situ formed living macro-alkoxyamines in the printed microstructures. Moreover, as a control experiment, surface modification was attempted on a bottom square prepared from PETA + BAPO without the addition of Nit-anthra. Unlike with Nit-anthra, the surface modification did not succeed even once, using TMPTA alone under irradiation at 800 nm, further proving the functionalization via NMP2 where Nit-anthra plays a key role. One major advantage of living polymerization—in situ NMP2 in this work—is the guaranteed covalent linkage between the surface-generated structures and the supporting layers.

Following the surface modification experiments on 2D microstructures, the functionalization of a 3D microstructure was carried out. As shown in Figure 2c, the functionalization was performed on the top of a cube using TMPTA ( $12.21 \text{ mW cm}^{-2}$  and 800 nm.). SEM image (Figure 2d) displays the “4D” pattern, highlighting the potential of our approach for precise control over surface functionality of 3D microstructures. Remarkably, the in situ NMP2 strategy can be easily adapted to commonly used wavelengths at 3D DLW (e.g., 800 nm, as used here) for both 3D micro-printing and surface functionalization, which is challenging for our previous method—photo-active alkoxyamine-based NMP2.

Prior to exploring the conditions for surface modification of microstructures, taking advantage of the adaptability of our photoresist to commercial DLP, we turned from light-control surface modification of microstructures to macrostructures. A flat, round piece (Figure 2e) with 8 mm diameter and  $275 \mu\text{m}$  thickness was made by DLP printing of a single layer ( $5 \text{ mW cm}^{-2}$  and 5 s). This simple geometry guarantees the compatibility of the macro-scale sample with the 3D DLW setup for precise surface modification (Figure 2e). The pattern—a map of France—was fabricated on the top of the round piece using TMPTA with Rhodamine B (RB) at  $11.39 \text{ mW cm}^{-2}$  ( $\lambda = 800 \text{ nm}$ ). RB was added to visualize the functionalized part via fluorescence lifetime imaging microscopy (FLIM). Finally, the FLIM image of the map (Figure 2e) demonstrates the successful spatial control of functionalization on the printed macrostructure.

### 2.3. Impact of Writing Conditions on Surface Modification

Having demonstrated the capability of in situ NMP2 for 3D printing and surface functionalization, here, we will focus on understanding the impact of various experimental conditions on surface modification of microstructures. All following experiments were carried out on the 3D DLW set up.

We started with determining the impact of laser wavelength and intensity applied for surface modification. Several groups of lines were fabricated on the top of a base square using pure TMPTA at three different wavelengths (780, 800, and 860 nm) with gradually increasing intensities (Figure 3a). This base square was made from our photoresist (Nit-anthra + BAPO + PETA) at 800 nm and fixed laser intensity ( $5.15 \text{ mW cm}^{-2}$ ). The heights of lines measured from AFM scans (Figure S4, Supporting Information) are plotted against laser intensity in Figure 3b. It clearly shows that the heights of lines increase with an increasing laser intensity at each wavelength, for example, at  $\lambda = 800 \text{ nm}$ , the heights increase from  $77 (\pm 17)$  to  $601 (\pm 16) \text{ nm}$  when the laser intensities vary from  $3.6$  to  $32.7 \text{ mW cm}^{-2}$ . Moreover, wavelengths have a strong influence on the heights of lines. One can notice that at the same intensity, the height of lines decreases with longer wavelengths, for instance, from  $\approx 650$  ( $\lambda = 780 \text{ nm}$ ) and  $\approx 420$  ( $\lambda = 800 \text{ nm}$ ) to  $\approx 140 \text{ nm}$  ( $\lambda = 860 \text{ nm}$ ) at  $19.0 \text{ mW cm}^{-2}$ . This can be explained by the plot of  $1/P_{\text{th}}^2$  against wavelength for surface modification (Figure S5, Supporting Information).<sup>[16]</sup>  $P_{\text{th}}$  is the threshold power defined as the minimum power required to initiate two-photon polymerization in DLW. Here, the value of  $1/P_{\text{th}}^2$  indicates the efficiency of two-photon polymerization induced by the in situ formed alkoxyamine. More detailed information on the reason to use the  $1/P_{\text{th}}^2$  plot and how to experimentally determine  $P_{\text{th}}$  is provided in the Supporting Information. As shown in Figure S5, Supporting Information, the value of  $1/P_{\text{th}}^2$  at  $\lambda = 780 \text{ nm}$  is larger than that at 800 nm and decreases further at 860 nm, indicating that the efficiency of two-photon polymerization for surface modification at  $780 \text{ nm} > 800 \text{ nm} > 860 \text{ nm}$ , which explains the observed trends of the heights of lines made at these wavelengths. Notably, our in situ NMP2 approach enables the successful surface modification upon

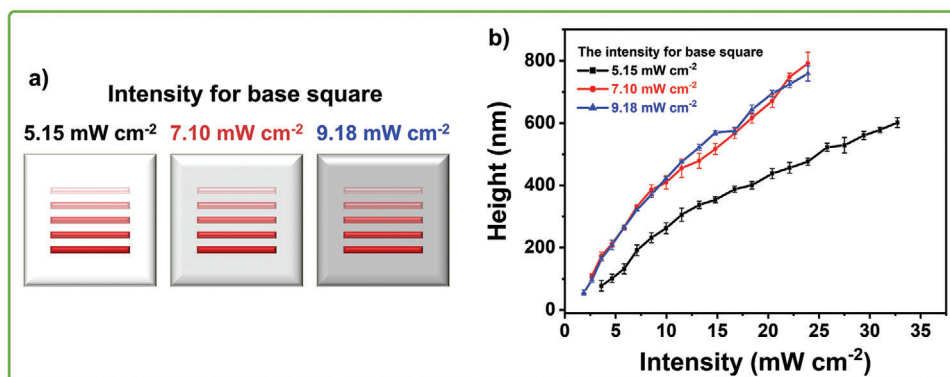


**Figure 4.** a) Schematic illustration of surface modifications to study the impact of the intensity used to fabricate the base square; b) Heights of lines fabricated at different intensities made from TMPTA alone at 800 nm under N<sub>2</sub> on the top of bottom squares made at 5.15, 7.10, and 9.18 mW cm<sup>-2</sup> (all at 800 nm). The bottom squares were made from PETA + Nit-anthra (2 wt%) + BAPO (2 wt%).

irradiation at 860 nm, which is far beyond the wavelength limit for surface modification of our previous NMP2 approach (maximum 760 nm). In addition, the successful surface modification at 860 nm further demonstrates the critical role of Nit-anthra in our approach, since the modification on a base square made solely from BAPO + PETA cannot be achieved at 800 nm (vide supra), let alone 860 nm.

Next, we studied how writing parameters used for the fabrication of the microstructure impact surface modification. For this purpose, several groups of lines made from TMPTA alone at 800 nm were fabricated on the top of three squares made from our formulation (Nit-anthra + BAPO + PETA) at 800 nm with different intensities (5.15, 7.10, and 9.18 mW cm<sup>-2</sup>) (see Figure 4a). As shown in Figure 4b, for each base square, the heights of lines measured from the AFM images (Figure S6, Supporting Information) were plotted against the intensities used for the lines' fabrication. Similar as above, irrespective of the base square the lines are generated upon, the heights of lines increase with increasing intensity applied for the lines' fabrication. Surprisingly, at the same intensity for lines' fabrication, increasing the intensity used for the base square from 5.15 to 7.10 mW cm<sup>-2</sup>, the heights of lines increase; while continuing to increase the intensity from 7.10 to 9.18 mW cm<sup>-2</sup>, the heights of lines remain similar. For instance, at 9.97 mW cm<sup>-2</sup> for modification, the heights of lines change from 263 (±17) to 409 (±21) nm, then to 423 (±6) nm, when intensities used for base squares increase from 5.15 mW cm<sup>-2</sup> to 7.10 mW cm<sup>-2</sup>, then to 9.18 mW cm<sup>-2</sup>. These observations differ significantly from those in our previous work—photo-alkoxyamine-based NMP2 for surface modification—where the lines' heights decrease with increasing laser intensity used for base square fabrication. We may assume that in our in situ NMP2 approach, a higher intensity used for the base square fabrication promotes the formation of macro-alkoxyamines, therefore further benefiting the surface modification; while above a certain intensity, the amount of macro-alkoxyamine will reach saturation. The positive correlations between the heights of functional layers with laser intensity used for microstructure fabrication and for surface modification simplify the implementation of 3D printing and surface functionalization.

Successive surface modification on microstructures has been well demonstrated in section 2.2. In order to gain a better understanding of this process, it is important to investigate the impact of writing conditions employed for the surface modification on the different functional layers. Therefore, as illustrated in Figure 5a, lines made at different intensities ( $\lambda = 800$  nm, TMPTA alone) were fabricated on the top of first and second squares. The first square was made from our formulation at 7.10 mW cm<sup>-2</sup> ( $\lambda = 800$  nm), the second from TMPTA alone at 8.02 mW cm<sup>-2</sup> ( $\lambda = 800$  nm). Figure 5b shows that the heights of lines (measured from AFM images in Figure S7, Supporting Information) increase with increasing intensity on the top of both the first and second layer. Meanwhile, it is also evident that at the same intensity, the lines on the top of the first layer are higher than those on the top of the second layer. Over the whole range of laser intensity employed for surface modification, the heights of lines on the top of the first layer are tunable from  $\approx 100$  to 800 nm, while the heights on the top of the second layer only vary from 60 to 275 nm. This is likely due to the formation of dead polymer chains during the in situ formation of alkoxyamine and NMP2 as evidenced for enhanced spin capturing polymerization and NMP in solution and bulk in addition to the low mobility of macroradicals over the various layers,<sup>[12b-d,13a,b]</sup> which deserves to be further studied in order to optimize such successive functionalization.

Indeed, these detailed studies of the impact of writing parameters lay a solid foundation for precisely controlled surface customization in 3D printing.

### 3. Conclusion

In summary, we proposed a new strategy—in situ NMP2—for the facilitation of light-based 3D printing and post-printing surface modification. The successful implementation of this strategy is based on the use of a novel photoresist containing a commercial photoinitiator BAPO and an easily synthesized Nit-anthra. Well-defined 3D microstructures were fabricated at a commonly used wavelength ( $\lambda = 800$  nm), demonstrating the compatibility of this photoresist with 3D DLW. Importantly, the surfaces of these microstructures can be precisely and successively modified via light, which is attributed to the addition of BAPO and Nit-anthra in the photoresist, allowing the in situ formation of

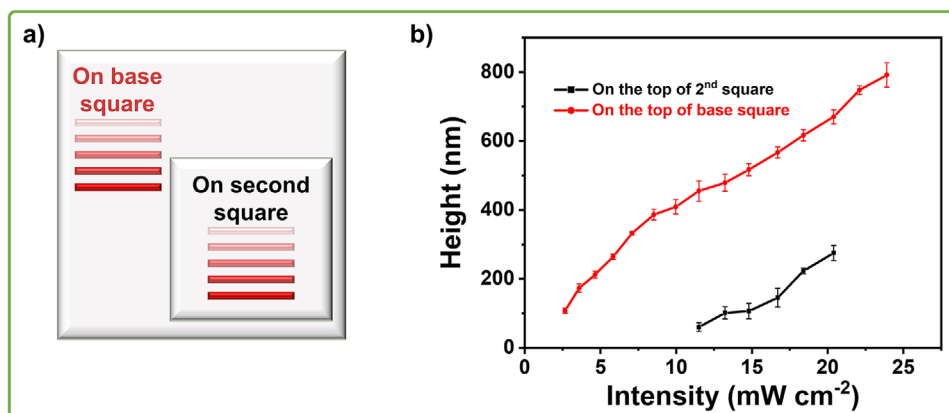


**Figure 5.** a) Schematic illustration of surface modifications on the base square as well as on the second square; b) Heights of lines fabricated at different intensities made from TMPTA alone on the top of first and second layer under N<sub>2</sub>. The first layer is a square made at 7.10 mW cm<sup>-2</sup> at 800 nm (PETA + Nit-anthra [2 wt%] + BAPO [2 wt%]). The second layer was made from TMPTA alone at 8.02 mW cm<sup>-2</sup> and 800 nm, under N<sub>2</sub>.

photo-active macro-alkoxyamine. Moreover, by adjusting writing conditions including light wavelength and intensity, the surface modification can be well manipulated. Remarkably, in our approach, precise surface modification can be conducted in a wide range of wavelengths, up to 860 nm, which is unattainable using our previous method—alkoxyamine-based NMP2. In addition, thanks to the simple preparation and facile scale-up of the photoresist, our strategy has been successfully extended to DLP-based 3D macro-printing and subsequent surface functionalization. *in situ* NMP2—this newly established and powerful approach—will undoubtedly accelerate the development of both micro- and macro-scale “living” 3D printing, which holds great promise for various applications, such as scaffolds and microfluidics.

## Supporting Information

Supporting Information is available from the Wiley Online Library or from the author.

## Acknowledgements

This work was supported by a French government grant managed by ANR under the France 2030 program (Project Mat-Light 4.0 – ANR-21-EXES-0012) and by the Interdisciplinary Institute HiFunMat, as part of the ITI 2021–2028 program of the University of Strasbourg, CNRS and Inserm, was supported by the IdEx Unistra (ANR-10-IDEX-0002) and the SFRI (STRAT<sup>US</sup> project, ANR-20-SFRI-0012) under the framework of the French Investments for the Future Program. The authors acknowledge the financial support provided by the Agence Nationale de la recherche (Project 2PhotonInsight ANR-16-CE08-0020-01, Project 3D CustomSurf ANR-19-CE06-0027, and Project Mat-Light 4.0 ANR-21-EXES-0012) as well as thank the support from the Institut Carnot MICA and from the Région Grand Est (Institutional Research Grant (MIPPI4D)).

## Conflict of Interest

The authors declare no conflict of interest.

## Data Availability Statement

The data that support the findings of this study are available from the corresponding author upon reasonable request.

## Keywords

3D printing, direct laser writing, nitroxide-mediated radical polymerization, photo-controlled reversible-deactivation radical polymerization, photopolymerization, photoresists, surface modification

Received: October 5, 2023  
Revised: November 16, 2023  
Published online:

- [1] a) C. W. Hull, US 638905, 1984. b) S. Maruo, O. Nakamura, S. Kawata, *Opt. Lett.* **1997**, 22, 132; c) M. Layani, X. Wang, S. Magdassi, *Adv. Mater.* **2018**, 30, 1706344; d) A. Bagheri, J. Jin, *ACS Appl Polym Mater.* **2019**, 1, 593; e) C. Barner-Kowollik, M. Bastmeyer, E. Blasco, G. Delaittre, P. Müller, B. Richter, M. Wegener, *Angew. Chem., Int. Ed.* **2017**, 56, 15828; f) S. C. Ligon, R. Liska, J. Stampfl, M. Gurr, R. Mülhaupt, *Chem. Rev.* **2017**, 117, 10212; g) R. L. Truby, J. A. Lewis, *Nature.* **2016**, 540, 371; h) J. Li, C. Boyer, X. Zhang, *Macromol. Mater. Eng.* **2022**, 307, 2200010; i) K. Jung, N. Corrigan, M. Ciftci, J. T. Xu, S. E. Seo, C. J. Hawker, C. Boyer, *Adv. Mater.* **2020**, 32, 1903850.
- [2] a) Y. Lin, J. Xu, *Adv. Opt. Mater.* **2018**, 6, 1701359; b) H. Ceylan, I. C. Yasa, O. Yasa, A. F. Tabak, J. Giltinan, M. Sitti, *ACS Nano.* **2019**, 13, 3353; c) O. Kufelt, A. El-Tamer, C. Sehring, S. Schlie-Wolter, B. N. Chichkov, *Biomacromolecules.* **2014**, 15, 650; d) M. Hippler, K. Weißenbruch, K. Riehler, E. D. Lemma, M. Nakahata, B. Richter, C. Barner-Kowollik, Y. Takashima, A. Harada, E. Blasco, M. Wegener, M. Tanaka, M. Bastmeyer, *Sci. Adv.* **2020**, 6, eabc2648; e) Y. Liu, H. Wang, J. Ho, R. C. Ng, R. J. H. Ng, V. H. Hall-Chen, E. H. H. Koay, Z. Dong, H. Liu, C.-W. Qiu, J. R. Greer, J. K. W. Yang, *Nat. Commun.* **2019**, 10, 4340; f) H. Zeng, P. Wasylczyk, C. Parmeggiani, D. Martella, M. Buresi, D. S. Wiersma, *Adv. Mater.* **2015**, 27, 3883; g) L. Cai, G. Chen, B. Su, M. He, *Chem. Eng. J.* **2021**, 426, 130545; h) J. A. Wilson, D. Luong, A. P. Kleinfehn, S. Sallam, C. Wesdemiotis, M. L. Becker, *J. Am. Chem. Soc.* **2018**, 140, 277; i) Q. Mu, L. Wang, C. K. Dunn, X. Kuang, F. Duan, Z. Zhang, H. J. Qi, T. Wang, *Addit. Manuf.* **2017**, 18, 74.
- [3] a) A. M. Greiner, B. Richter, M. Bastmeyer, *Macromol. Biosci.* **2012**, 12, 1301; b) B. Richter, T. Pauloehrl, J. Kaschke, D. Fichtner, J. Fischer, A. M. Greiner, D. Wedlich, M. Wegener, G. Delaittre, C. Barner-Kowollik, M. Bastmeyer, *Adv. Mater.* **2013**, 25, 6117; c) J. Zhang, H. Ding, X. Liu, H. Gu, M. Wei, X. Li, S. Liu, S. Li, X. Du, Z. Gu, *Small.* **2021**, 17, 2101048; d) H. Ceylan, I. C. Yasa, M. Sitti, *Adv. Mater.* **2017**, 29, 1605072; e) R. A. Farrer, C. N. Lafratta, L. Li, J. Praino, M. J.

- Naughton, B. E. A. Saleh, M. C. Teich, J. T. Fourkas, *J. Am. Chem. Soc.* **2006**, *128*, 1796; f) A. P. Kleinfehn, J. A. L. Lindemann, A. Razvi, P. Philip, K. Richardson, K. Nettleton, M. L. Becker, D. Dean, *Biomacromolecules*. **2019**, *20*, 4345; g) G. Gonzalez, A. Chiappone, K. Dietliker, C. F. Pirri, I. Roppolo, *Adv. Mater. Technol.* **2020**, *5*, 2000374; h) N. Azim, J. F. Orrico, D. Appavoo, L. Zhai, S. Rajaraman, *RSC Adv.* **2022**, *12*, 25605.
- [4] Y. Gu, J. Zhao, J. A. Johnson, *Trends Chem.* **2019**, *1*, 318.
- [5] a) A. S. Quick, J. Fischer, B. Richter, T. Pauloehrl, V. Trouillet, M. Wegener, C. Barner-Kowollik, *Macromol. Rapid Commun.* **2013**, *34*, 335; b) A. S. Quick, H. Rothfuss, A. Welle, B. Richter, J. Fischer, M. Wegener, C. Barner-Kowollik, *Adv. Funct. Mater.* **2014**, *24*, 3571; c) D. W. Yee, M. D. Schulz, R. H. Grubbs, J. R. Greer, *Adv. Mater.* **2017**, *29*, 1605293; d) A. S. Quick, A. De Los Santos Pereira, M. Bruns, T. Bückmann, C. Rodriguez-Emmenegger, M. Wegener, C. Barner-Kowollik, *Adv. Funct. Mater.* **2015**, *25*, 3735; e) I. Roppolo, F. Frascella, M. Gastaldi, M. Castellino, B. Ciubini, C. Barolo, L. Scaltrito, C. Nicosia, M. Zanetti, A. Chiappone, *Polym. Chem.* **2019**, *10*, 5950.
- [6] T. K. Claus, B. Richter, V. Hahn, A. Welle, S. Kayser, M. Wegener, M. Bastmeyer, G. Delattre, C. Barner-Kowollik, *Angew. Chem., Int. Ed.* **2016**, *55*, 3817.
- [7] a) A. Bagheri, C. M. Fellows, C. Boyer, *Adv. Sci.* **2021**, *8*, 2003701; b) V. A. Bobrin, J. Zhang, N. Corrigan, C. Boyer, *Adv. Mater. Technol.* **2022**, *8*, 2201054; c) M. Chen, Y. Gu, A. Singh, M. Zhong, A. M. Jordan, S. Biswas, L. T. J. Korley, A. C. Balazs, J. A. Johnson, *ACS Cent. Sci.* **2017**, *3*, 124.
- [8] A. Bagheri, K. E. Engel, C. W. A. Bainbridge, J. Xu, C. Boyer, J. Jin, *Polym. Chem.* **2020**, *11*, 641.
- [9] a) Z. Zhang, N. Corrigan, A. Bagheri, J. Jin, C. Boyer, *Angew. Chem., Int. Ed.* **2019**, *58*, 17954; b) A. Bagheri, C. W. A. Bainbridge, K. E. Engel, G. G. Qiao, J. Xu, C. Boyer, J. Jin, *ACS Appl. Polym. Mater.* **2020**, *2*, 782; c) C. W. A. Bainbridge, K. E. Engel, J. Jin, *Polym. Chem.* **2020**, *11*, 4084; d) K. Lee, N. Corrigan, C. Boyer, *Angew. Chem., Int. Ed.* **2021**, *60*, 8839.
- [10] X. Wu, B. Gross, B. Leuschel, K. Mougin, S. Dominici, S. Gree, M. Belqat, V. Tkachenko, B. Cabannes-Boué, A. Chemtob, J. Poly, A. Spangenberg, *Adv. Funct. Mater.* **2021**, *32*, 2109446.
- [11] a) M. Belqat, X. Wu, J. Morris, K. Mougin, T. Petithory, L. Pieuchot, Y. Guillauneuf, D. Gigmes, J.-L. Clément, A. Spangenberg, *Adv. Funct. Mater.* **2023**, *33*, 2211971; b) L. Qiao, M. Zhou, G. Shi, Z. Cui, X. Zhang, P. Fu, M. Liu, X. Qiao, Y. He, X. Pang, *J. Am. Chem. Soc.* **2022**, *144*, 9817; c) Y. Jia, C. A. Spiegel, A. Welle, S. Heißler, E. Sedghamiz, M. Liu, W. Wenzel, M. Hackner, J. P. Spatz, M. Tsotsalas, E. Blasco, *Adv. Funct. Mater.* **2023**, *33*, 2207826; d) X. Shi, V. A. Bobrin, Y. Yao, J. Zhang, N. Corrigan, C. Boyer, *Angew. Chem., Int. Ed.* **2022**, *61*, e202206272.
- [12] a) V. Sciannamea, C. Guerrero-Sanchez, U. S. Schubert, J.-M. Catala, R. Jérôme, C. Detrembleur, *Polymer*. **2005**, *46*, 9632; b) E. H. H. Wong, T. Junkers, C. Barner-Kowollik, *J. Polym. Sci., Part A: Polym. Chem.* **2008**, *46*, 7273; c) V. Sciannamea, R. Jérôme, C. Detrembleur, *Chem. Rev.* **2008**, *108*, 1104; d) C. Dommanget, C. Boisson, B. Charleux, F. D'agosto, V. Monteil, F. Boisson, T. Junkers, C. Barner-Kowollik, Y. Guillauneuf, D. Gigmes, *Macromolecules*. **2013**, *46*, 29.
- [13] a) Y. Guillauneuf, D. Bertin, D. Gigmes, D.-L. Versace, J. Lalevée, J.-P. Fouassier, *Macromolecules*. **2010**, *43*, 2204; b) D.-L. Versace, J. Lalevée, J.-P. Fouassier, Y. Guillauneuf, D. Bertin, D. Gigmes, *Macromol. Rapid Commun.* **2010**, *31*, 1383; c) G. Audran, E. G. Bagryanskaya, S. R. A. Marque, P. Postnikov, *Polymers*. **2020**, *12*, 1481; d) S. Telitel, J. C. Morris, Y. Guillauneuf, J.-L. Clément, F. Morlet-Savary, A. Spangenberg, J.-P. Malval, J. Lalevée, D. Gigmes, O. Soppera, *ACS Appl. Mater. Interfaces*. **2020**, *12*, 30779.
- [14] a) W. Haske, V. W. Chen, J. M. Hales, W. Dong, S. Barlow, S. R. Marder, J. W. Perry, *Opt. Express*. **2007**, *15*, 3426; b) T. Frenzel, M. Kadic, M. Wegener, *Science*. **2017**, *358*, 1072; c) M. Hippler, E. Blasco, J. Qu, M. Tanaka, C. Barner-Kowollik, M. Wegener, M. Bastmeyer, *Nat. Commun.* **2019**, *10*, 232; d) A. Balena, M. Bianco, F. Pisanello, M. De Vittorio, *Adv. Funct. Mater.* **2023**, *33*, 2211773; e) C. N. Lafratta, J. T. Fourkas, T. Baldacchini, R. A. Farrer, *Angew. Chem., Int. Ed.* **2007**, *46*, 6238.
- [15] a) B. Zhang, K. Kowsari, A. Serjouei, M. L. Dunn, Q. Ge, *Nat. Commun.* **2018**, *9*, 1831; b) Z. Zhao, X. Tian, X. Song, *J. Mater. Chem. C*. **2020**, *8*, 13896.
- [16] a) T. Baldacchini, C. N. Lafratta, R. A. Farrer, M. C. Teich, B. E. A. Saleh, M. J. Naughton, J. T. Fourkas, *J. Appl. Phys.* **2004**, *95*, 6072; b) M. Jin, H. Hong, J. Xie, J.-P. Malval, A. Spangenberg, O. Soppera, D. Wan, H. Pu, D.-L. Versace, T. Leclerc, P. Baldeck, O. Poizat, S. Knopf, *Polym. Chem.* **2014**, *5*, 4747.